A general approach to model interfaces using existing soil constitutive models - application to hypoplasticity

H. Stutz[1], D. Mašín, A.S. Sattari and F. Wuttke

H. Stutz
Marine and Land Geotechnics / Geomechanics, Institute for Geoscience, Kiel University, Ludewig–Meyn–Str. 10, 24321 Kiel, Germany
Tel.: +49-880-1979
Email:hs@gpi.uni-kiel.de

D. Mašín
Faculty of Science, Charles University in Prague, Albertov 6, 12843 Prague 2, Czech Republic
Email: Masin@natur.cuni.cz

A.S. Sattari & F. Wuttke
Marine and Land Geotechnics / Geomechanics, Institute for Geoscience, Kiel University, Ludewig–Meyn–Str. 10, 24321 Kiel, Germany
Email:sattari@gpi.uni-kiel.de ; fw@gpi.uni-kiel.de

Accepted for publication in *Computers and Geotechnics* (10.02.2017); doi: 10.1016/j.compgeo.2017.02.010

[1]corresponding author

1. INTRODUCTION

The modelling of interfaces is a challenging topic in geotechnical engineering. Advanced and specialised constitutive interface models should be used to realistically simulate soil-structure contact behaviour [1, 2]. There are few numerical and constitutive models that adequately consider interface behaviour.
From the late seventies to nowadays, numerical techniques for interface modelling various [3, 4, 5, 6, 7, 8, 9, 10, 11, 12, 13, 14, 15] have been developed. To properly represent the interface, it is essential to use a suitable constitutive model. The simplified constitutive Mohr-Coulomb frictional model is often used. Various soil-structure interface models from non-linear elasticity [16, 17], elasto-plastic models [18, 19, 20, 21, 22], state-dependent plasticity models [23, 24, 25, 26], models using damage mechanics [27], and disturbed state concept models [28, 29, 30] have been proposed. There is only a limited number of 3D interface constitutive interface models [31, 20, 32, 27, 33, 34, 35, 36]. The method proposed in this paper will overcome the problem of availability and implementation using a simple and robust approach. Recently published hypoplastic interface models [35, 37] have been implemented using the new approach. Weißenfels and Wriggers [9] developed a projection method to integrate plasticity models into a mixed mortar formulation. In contrast, the goal of our method is to define an approach that can be adapted to constitutive interface modelling with the mortar method using existing 3D constitutive soil models.
In order to make such advanced models available, the whole constitutive model (here UMAT subroutine in ABAQUS [38]) is used, and the 3D model is modified so that surface roughness is accounted for. The necessary tensor entries are provided by the frictional subroutine (FRIC keyword in ABAQUS) to call the user-defined material subroutine (UMAT). This approach minimises the effort required to implement an adequate constitutive interface model.
The theoretical rationale is the hypothesis that the soil in the interface has the same deformation behaviour as the soil continuum surrounding the interface [39, 40]. This hypothesis was also used when developing the enhanced hypoplastic interface models proposed by Stutz et al. [35, 37, 41].
After briefly introducing the hypoplastic interface models, the stress and strain rate tensor assumptions are explained, and the implementation approach is introduced. This is followed by a verification of the finite element analysis with Gauss point calculation [35, 37]. The new model is is used to simulate a large interface shear device [42] and compared to the results of the experimental data.

2. HYPOPLASTIC INTERFACE MODELS

The hypoplastic interface models has already been applied to fine-grained soils [37], and the enhanced hypoplastic model has been applied to granular soil structure interfaces [35]. The underlying assumptions are introduced below. The interface model formulations are based on the clay hypoplastic model [43] and the granular hypoplastic model [44], which can be found in Appendix B and Appendix C.

2.1. Reduced stress and strain rate tensors

The original hypoplastic models can be used without modifying the tensorial equations [35, 37]. The mathematical operators will be modified so that the model can be used with a reduced stress tensor in the Voigt notation as:

$$\boldsymbol{\sigma}^h = \begin{bmatrix} \sigma_{11} & \sigma_{12} & \sigma_{13} \\ \sigma_{21} & \sigma_{22} & \sigma_{23} \\ \sigma_{31} & \sigma_{32} & \sigma_{33} \end{bmatrix} \Rightarrow \begin{bmatrix} \sigma_n & \tau_x & \tau_y \\ \tau_x & \sigma_p & 0 \\ \tau_y & 0 & \sigma_p \end{bmatrix} \tag{1}$$

where $\boldsymbol{\sigma}^h$ denotes the whole stress tensor, and the degenerated vectorial form $\boldsymbol{\sigma}$ is:

$$\boldsymbol{\sigma} = \begin{bmatrix} \sigma_n \\ \sigma_p \\ \tau_x \\ \tau_y \end{bmatrix} \tag{2}$$

A brief comment for the in-plane stress σ_p: at the start of each simulation, the stress initialization is done by $\sigma_p = \sigma_n$. After the initialization, the normal and in-plane stresses are developed independently of each other.
The strain rate tensor $\dot{\boldsymbol{\varepsilon}}$ is defined as:

$$\dot{\boldsymbol{\varepsilon}}^h = \begin{bmatrix} \dot{\varepsilon}_{11} & \dot{\varepsilon}_{12} & \dot{\varepsilon}_{13} \\ \dot{\varepsilon}_{21} & \dot{\varepsilon}_{22} & \dot{\varepsilon}_{23} \\ \dot{\varepsilon}_{31} & \dot{\varepsilon}_{32} & \dot{\varepsilon}_{33} \end{bmatrix} \Rightarrow \begin{bmatrix} \dot{\varepsilon}_n & \frac{\dot{\gamma}_x}{2} & \frac{\dot{\gamma}_y}{2} \\ \frac{\dot{\gamma}_x}{2} & 0 & 0 \\ \frac{\dot{\gamma}_y}{2} & 0 & 0 \end{bmatrix} \tag{3}$$

where, $\dot{\boldsymbol{\varepsilon}}^h$ denotes the hole strain rate tensor, $\dot{\epsilon}_n$ the normal strain rate and $\frac{\dot{\gamma}_x}{2}$, $\frac{\dot{\gamma}_y}{2}$ the shear strain rate in the x and y direction, respectively. The vectorial form $\dot{\boldsymbol{\varepsilon}}$ is defined as:

$$\dot{\boldsymbol{\varepsilon}} = \begin{bmatrix} \dot{\varepsilon}_t \\ 0 \\ \frac{\dot{\gamma}_x}{2} \\ \frac{\dot{\gamma}_y}{2} \end{bmatrix} \tag{4}$$

The in-plane components of the strain rate tensor are $\varepsilon_p = 0$. For the use of the in-plane strain, $\dot{\varepsilon}_p = 0$, and for the in-plane stress, $\sigma_p \neq 0$. Using these modified stress and strain tensors will lead to simple shear stress and strain conditions at the interface [45, 46]. These stress and strain tensors will lead to odeometric stress and strain assumption at the interface. More information about the initialization of σ_p are given in Stutz and Mašín [37]. These reduced versions are used in conjunction with the mathematical operators defined in Appendix A.

2.2. Fine-grained hypoplastic interface model

The fine-grained hypoplastic interface model is based on the hypoplastic soil model with explicit defined asymptotic states of Mašín [43]. The general form of the hypoplastic model [47] is:

$$\dot{\boldsymbol{\sigma}} = f_s \left(\boldsymbol{L} : \dot{\boldsymbol{\varepsilon}} + f_d \boldsymbol{N} \|\dot{\boldsymbol{\varepsilon}}\| \right), \tag{5}$$

where $\dot{\boldsymbol{\varepsilon}}$ and $\dot{\boldsymbol{\sigma}}$ are the strain and stress rate tensors, respectively. $\boldsymbol{L}$ and $\boldsymbol{N}$ are the fourth- and second-order constitutive tensors, f_s is a factor that controls the influence of the mean stress (barotropy) and f_d is a factor for the influence of the relative density (pyknotropy). Mašín [48] proposed an alternative expression for the hypoplastic clay model developed from the general form of the hypoplastic constitutive formula [47]:

$$\dot{\boldsymbol{\sigma}} = f_s \boldsymbol{L} : \dot{\boldsymbol{\varepsilon}} - \frac{f_d}{f_d^A} \boldsymbol{A} : \boldsymbol{d} \|\dot{\boldsymbol{\varepsilon}}\|, \tag{6}$$

where $\boldsymbol{d}$ is the asymptotic strain rate direction and f_d^A describes the value of f_d at the asymptotic state boundary surface. $\boldsymbol{A}$ is defined as:

$$\boldsymbol{A} = f_s \boldsymbol{L} + \frac{\boldsymbol{\sigma}}{\lambda^*} \otimes \mathbf{1}, \tag{7}$$

where λ^* is a model parameter. Equation (6) enables the use and incorporation of an appropriate arbitrary shape for the asymptotic shape boundary surface. This is done by specification of f_d^A in dependence of the void and stress ratio [48]. The formulation of the full model is given in Appendix C.

2.3. Granular hypoplastic interface model

Von Wolffersdorff [44] extended the basic formula of the hypoplastic model [47] by incorporating a predefined limit state surface from Matsuoka and Nakai [49]. The constitutive stress-strain equation is defined as:

$$\dot{\boldsymbol{\sigma}} = f_s \left(\boldsymbol{L} : \dot{\boldsymbol{\varepsilon}} + f_d \boldsymbol{N} \|\dot{\boldsymbol{\varepsilon}}\| \right), \tag{8}$$

The model is briefly described in Appendix B.

3. INNOVATIVE APPROACH FOR INTERFACE MODELLING

The model was implemented using the software package ABAQUS FEA [38]. However, the method proposed is not limited to a specific software package. It can thus be used in different codes and numerical techniques with simple modifications [4, 5].
Using ABAQUS, it is possible to define a user constitutive model for frictional behaviour (FRIC). This subroutine is implemented by the use of a mortar method that is a segment-to-segment approach defining a master and slave surfaces [50].
For clarification, the UMAT subroutine can be used for: "User subroutine to define the mechanical behaviour of a material". The FRIC subroutine can be used for:" User subroutine to define frictional behaviour for contact surfaces ". Additional information about both subroutines is provided in the ABAQUS documentation [50].
In the finite element method, interface models are generally implemented with the primary state variables stress and the strain rate normal to the interface (σ_n, $\dot{\varepsilon}_n$) and shear components (τ_x,τ_y,$\dot{\gamma}_x$,$\dot{\gamma}_y$). To incorporate the in-plane σ_p stress into the formulation as an additional state variable together with the void ratio e must be considered. This is done by an algorithm that will be introduced below. With respect to the use of a stretching tensor $\boldsymbol{D}$, the spin tensor $\boldsymbol{W}$ can be neglected because rigid body rotations are assumed.

Implementation scheme

The reduced tensor notation (Section 2) will be used in the FRIC subroutine. The tensor entries are transformed and transferred to the 3D UMAT implementation available from the soilmodel.info project [51]. The innovative approach is presented in Figure 1. In the actual time increment, the FRIC subroutine is invoked. The input of all necessary parameters, stresses and displacements are supplemented from the ABAQUS calculation kernel. The relative shear displacements u are transformed by the virtual shear zone thickness to shear strains ε_x; ε_y .
The input from the FRIC routine is formatted to match the UMAT input format and transferred to the UMAT subroutine, taking into consideration a normal strain rate of $\dot{\varepsilon}_n = 0$ for the first iteration. To ensure a volumetric behaviour according to the simple shear conditions, the normal contact stress rate $\dot{\sigma}_n^{Press}$ is used to find the appropriate normal strain rate $\dot{\varepsilon}_n$. This is done by using a Newton-Raphson iteration scheme. The interface contact stress rate is derived according to the normal deformation that must be chosen according to the stress contact rate $\dot{\sigma}_n^{Press}$. After the UMAT call, the relative error "*err.*" is compared to the tolerance (TOL). If the tolerance TOL is smaller than the error, a new value of the $\dot{\varepsilon}_n^{n+1}$ must be approximated using the Newton-Raphson algorithm until the condition of err $\leq TOL$ is fulfilled. The stresses $\boldsymbol{\sigma}_{UMAT}$ are transformed back to the stress definition by the FRIC subroutine $\boldsymbol{\sigma}_{FRIC}$. This procedure is used for each increment when the FRIC routine is used.
The scheme can be used with any kind of 3D constitutive model. Here, the hypoplastic fine-grained and granular interface models are used. This innovative approach can be used with different constitutive models by adapting the scheme. The Newton-Raphson method used to derive the normal strain rate and the virtual thickness approach is defined below.

Newton-Raphson method

The Newton-Raphson method (Figure 1) implemented to find the necessary normal contact strain in dependence of the normal stress rate, which is supplemented into the FRIC user subroutine from the ABAQUS kernel. The formula for the Newton-Raphson iteration is:

$$x_1 = x_0 - \frac{f(x_0)}{f'(x_0)}, \tag{9}$$

where x_1 is the new value of the desired value, x_0 is the initial estimate for the obtained value, f is the function used with x_0 and f' is the first derivative of the function with x_0 for the initial estimate.
This is repeated with the formula as:

$$x_{n+1} = x_n - \frac{f(x_n)}{f'(x_n)}, \tag{10}$$

until a certain error tolerance TOL is reached. The stability and efficiency of the method proposed for the given normal contact strain rate is demonstrated (Section 4). In the new approach, the following equation is used:

$$\dot{\varepsilon}_n^{n+1} = \dot{\varepsilon}_n^n - \frac{f(\dot{\varepsilon}_n^n)}{f'(\dot{\varepsilon}_n^n)}, \tag{11}$$

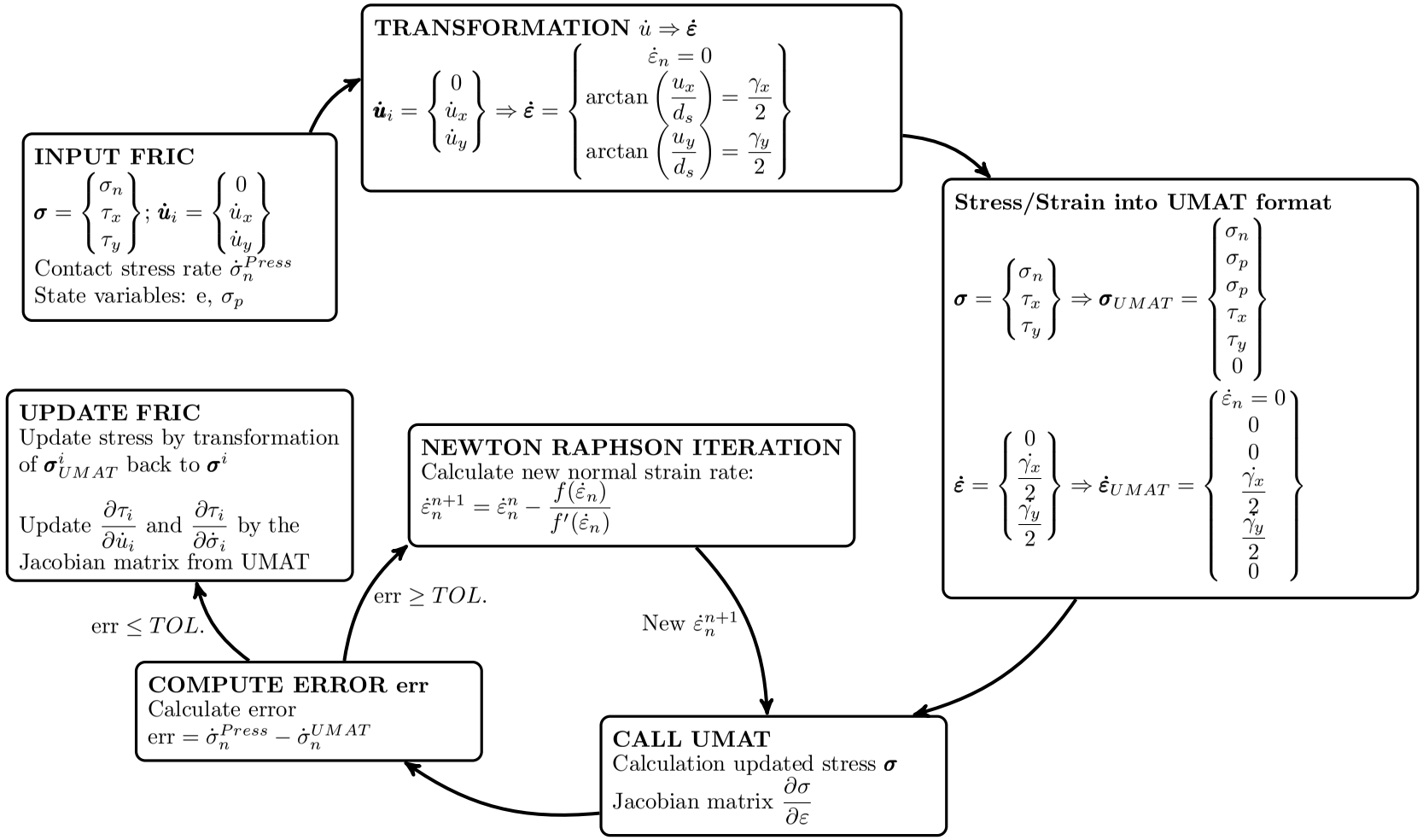

Figure 1: Implementation scheme for the FRIC subroutine using the UMAT subroutine

where f is the UMAT function call. In the UMAT, the first derivative is defined by the Jacobian matrix $\frac{\partial \sigma_n}{\partial \varepsilon_n}$ (Figure 1).

Virtual thickness approach

As mentioned by Gutjahr [52], the shear zone thickness is dependent on the shear strain and shear displacement. Arnold [53] discussed the possibility of using a virtual shear zone thickness to scale the relative displacements in the interface. Using this approach, it is possible to calibrate the shear stress evolution for experimental data. Similar approaches are used in other finite element packages. The shear strains in the asymptotic state [34, 35, 52] are defined by:

$$\tan \dot{\gamma}_i = \frac{u_i}{d_s^v}; \tag{12}$$

When using the real shear zone thickness, the increments must be small because otherwise the shear strain will dramatically increase. To prevent this, the virtual shear zone approach [54] is used. The product of the specific length of the contact face (CHRLENTGH) and the artificial multiplier t_i as a virtual shear zone thickness d_s is applied to overcome this problem.
The shear-zone thickness is introduced as the virtual shear zone thickness d_s^v:

$$d_s^v = t_i \cdot \text{CHRLENGTH}, \tag{13}$$

where CHRLENGTH is the ABAQUS keyword for the specific length of the contact face. The true shear zone thickness can be used but will be accompanied by the use of small increments and an increase in the computational time needed.The coarse and fine-grained models are verified below.

4. VERIFICATION OF IMPLEMENTATION

The approach proposed in Section 3 was verified using the parameter sets given in Table 1. Different aspects were studied:

- Comparison of Gauss-point simulations used a simple Euler forward integration with the finite element implementation using the new approach
- Study of the mesh sensitivity

Table 1: Parameters for the evaluation of HCC and HCE contact models

Hypoplastic granular model [55]		Hypoplastic clay model [43]	
Parameters	Value	Parameters	Value
φ_c	31	λ^*	0.095
h_s [kPa]	$1 \cdot 10^6$	κ^*	0.015
n	0.29	ν	0.1
e_{d0}	0.61	φ_c	21.9
e_{c0}	0.96	N	1.19
e_{i0}	1.09	κ_r	1.0
α	0.13		
β	2		

The interface shear test model used for verification is described below.

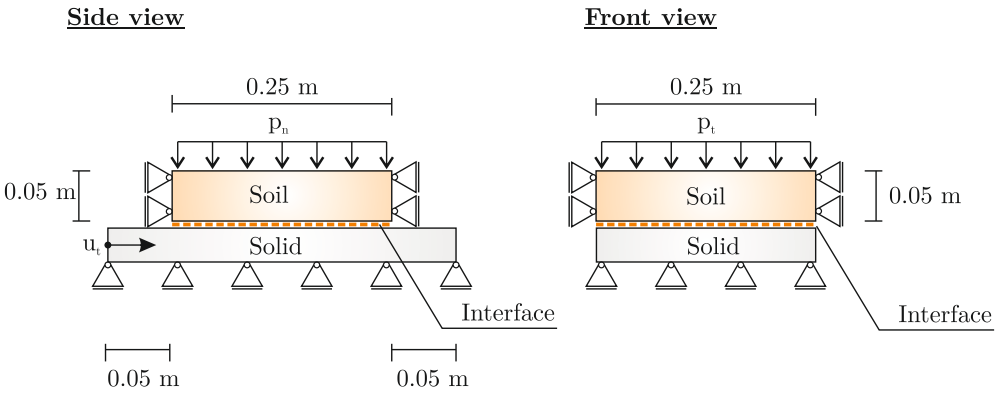

Figure 2: Geometry for direct shear verification simulation model adapted from Weißenfels et al. [8]

4.1. Description of the numerical direct shear interface test

The interface shear test model was introduced by Weißenfels et al. [8]. This model was modified to verify the approach described here. The model consist of: the soil and the continuum (Figure 2).
The soil sample have a dimension of 25 x 25 x 5 cm (Figure 2). The soil sample with the interface is applied over a structural part with the dimensions of 35 x 25 x 5 cm. The initial stress applied is p_n, and u_t is the shear displacement. This displacement was applied to all nodes of the structural part to model a homogeneous displacement field in the interface. The steel block was modelled as a linear elastic material with the following material constants: Young's modulus of $1 \cdot 10^{16}$ and Poisson's ratio of $\nu = 0.25$. The element type used was a linear interpolation of eight noded elements (Abaqus keyword: C3D8). The thick line indicates the interface that was modelled by a mortar method using the master and slave concept as described in the ABAQUS documentation [50]. The contact in the shear direction was modelled as described in Section 2. The normal contact was modelled with the augmented Lagrange technique [50]. These simulations were compared with the standard Mohr-Coulomb tangential contact formulation.
A geostatic stress field was applied (Step 1), a body force was applied to activate the unit weight of the soil sample (Step 2), and the shearing was initialised (Step 3). The applied final shear displacement is $u_t = 5$ cm.
First, the mesh size sensitivity was analysed. The Gauss point simulation and the finite element implementation were then verified.

4.2. Mesh sensitivity analysis

The three different meshes (Figure 3) were used together with the boundary value problem described above. The parameters from Table 1 were used to calculate the stress deformation behaviour of the interface test using different mesh-sizes.
The meshes consisted of different numbers of elements:

- coarse mesh size: 1 element
- intermediate mesh size: 128 elements
- fine mesh size: 507 elements

These different meshes were used to show that the behaviour and the response of the model will not be influenced by the subroutine and the results only differed slightly when different mesh sizes were used.
The normal pressure p_n was 200 kPa, and the interface was assumed to be completely rough ($\kappa_r = 1.0$). The results of this mesh sensitivity analysis are given for sand (Figure 4a). The results for the coarse mesh with one soil element under-predicted the peak behaviour. The intermediate and fine mesh showed similar results with small differences in the model response. For all different mesh sizes the same asymptotic shear stresses were reached under the final displacement of $u_t = 5$cm.
The clay mesh sensitivity analysis (Figure 4b) was assumed to be completely rough ($\kappa_r = 1.0$). The normal stress (p_n)

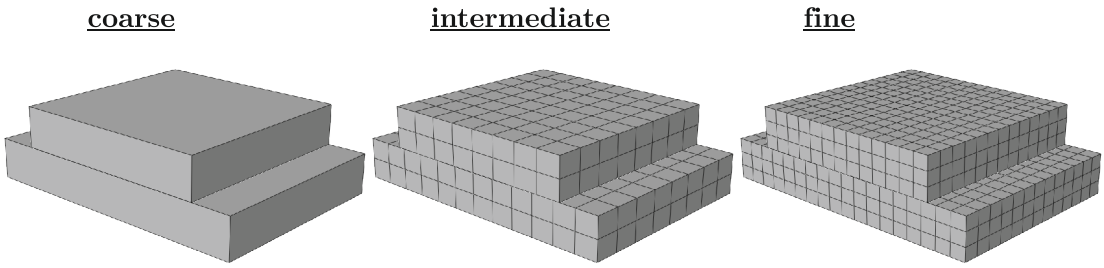

Figure 3: Three different mesh sizes from coarse, intermediate and fine mesh size used to simulate mesh sensitivity

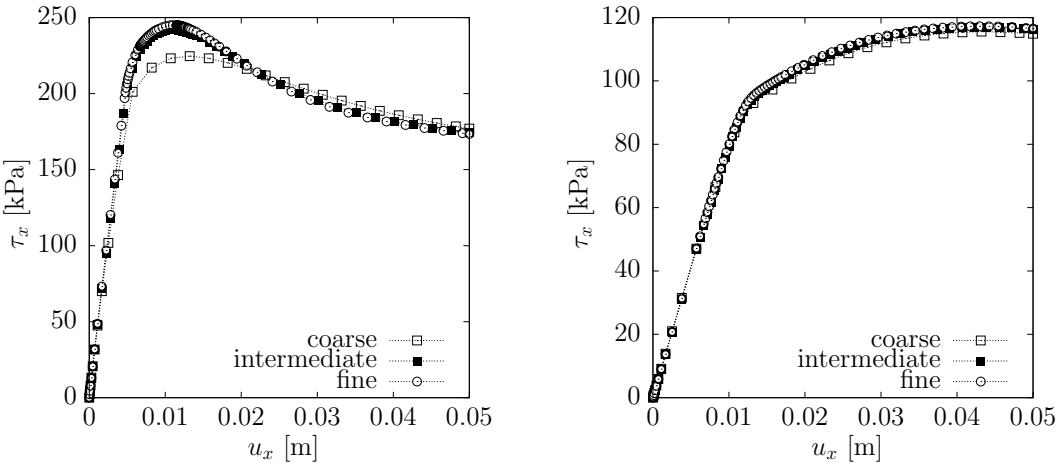

(a) (b)

Figure 4: Shear displacement u_x to shear stress τ_x graphs for mesh sensitivity analysis for (a) sand and (b) clay

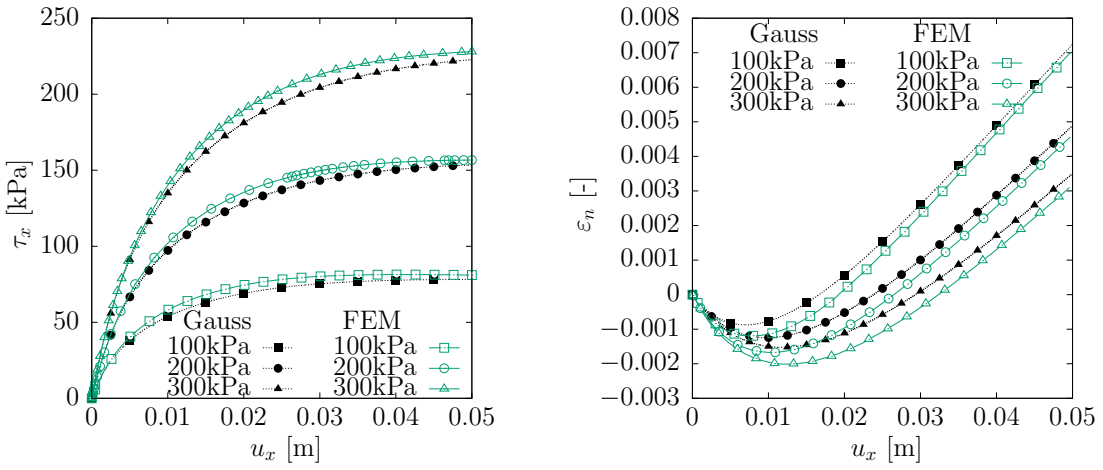

(a) u_x-τ_x (b) u_x-ε_n

Figure 5: Comparison between the Gauss point algorithm and the finite element implementation of the constitutive interface models for sand

was 100 kPa in all three simulations. The coarse mesh simulated slightly smaller shear stress around the peak than the intermediate and fine mesh. The different mesh sizes tend to show the same asymptotic shear stress behaviour. The two different mesh sensitivity analyses indicate that the mesh size did not influence the behaviour of the shear stress development. Subsequent analyses were therefore conducted with an intermediate mesh size. The verification based on the Gauss-point code and the ABAQUS results is described below.

4.3. Verification of coarse-grained soil-structure interface model

The implementation procedure and the accuracy in modelling with a granular enhanced hypoplastic interface model were verified for the different applied normal stresses (p_n) of 100, 200 and 300 kPa (Figure 5). The virtual shear zone thickness d_s^v was 1.0.

In all three different stresses, the finite element implementation slightly overpredicted the results compared with the Gauss point algorithm because of the numerical integration scheme used in the finite element implementation. However, the Gauss point solution can be treated as quasi-analytical solution with a tolerance of 0.0%. The soil sample overlaying the steel surface was also modelled with the hypoplastic 3D constitutive model of Von Wolffersdorff [44]. Because of the compression of the soil sample, vertical displacements led to the small differences in the shear stress evolution. When comparing of the results for the normal strain ε_n, the agreement between both solutions was sufficient. The slightly smaller strain can be explained by the normal soil deformation over the interface. In general, the agreement between both solutions was satisfactory.

4.4. Verification of fine-grained soil-structure interface model

The fine-grained interface model was verified using a normal stress (p_n) of 50, 100, 200 kPa. d_s^v was 1.0, and a completely rough interface ($\kappa_r = 1.0$) was assumed (Figure 6).

The same shear behaviour trend as for the granular interface model was observed. Compared with the Gauss point simulation, there was a slight overprediction of the finite element solution. The only exception was the slight underprediction of the shear stress for the simulation with a pressure of $p_n = 50$ kPa, which was detectable after a shear deformation of $u_t = 3$ cm. This was because of the number of maximum steps for the Newton-Raphson iteration scheme. At $u_t = 3$ cm, the iteration scheme reach the maximum number of iterations. This led to an disagreement between the calculated stress rate and the normal stress rate provided by the FRIC subroutine. There was also a small difference for the direct interface shear simulation.

The behaviour of the volumetric normal strain ε_n is shown in Figure 6b. The trend for all different models was comparable, but the simulations done with the finite element method showed a contractive behaviour because the soil behaviour above the interface was modelled by the hypoplastic fine-grained soil model. This led to an inhomogeneous stress at the interface when comparing in both solutions. The semi-analytical solution used a constant stress.

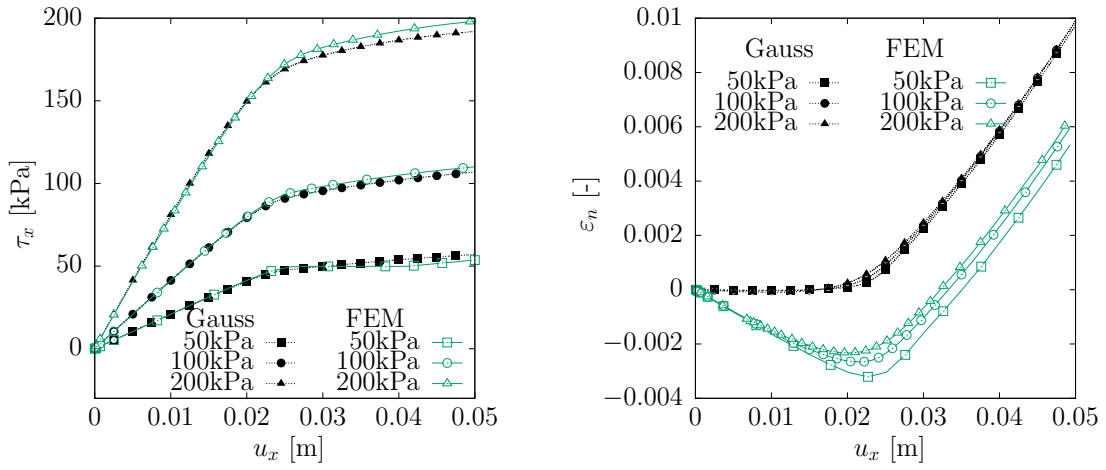

(a) u_x-τ_x (b) u_x-ε_n

Figure 6: Comparison between the Gauss point algorithm and the finite element implementation of the constitutive interface models for clay

In the finite element calculation, the overlaying soil acted as a spring stiffness [56, 57]. Below, the standard built-in Mohr-Coulomb model will be compared with the enhanced hypoplastic granular interface model.

4.5. Comparison of Mohr-Coulomb and hypoplastic constitutive interface model

For demonstration purpose, the two completely rough granular interface simulations are compared using the boundary value problem of the direct interface shear test (Section 4.1). The first simulation was conducted with the Mohr-Coulomb friction model that was a default model for simulations, taking into consideration interfaces. The second simulation used the hypoplastic model [44] with the new approach for the interface. In both simulations, the soil was modelled by the hypoplastic model [44] with the parameter for Hostun sand (Table 1).
The Mohr-Coulomb default model needs only the friction coefficient, which was set to $\mu = 1.0$ for completely rough conditions. Both the shear stress τ_x to the shear displacement u_x were simulated (Figure 7).
The shear stress that developed in the soil mass was 2–3 times smaller for the enhanced hypoplastic interface model than for the Mohr-Coulomb model. Applying the enhanced hypoplastic interface model led to the continuous development of shear stresses along the interface in contrast to the Mohr-Coulomb model.
This explains that the overall behaviour is not really different as expected from the comparison of the shear stress field (Figure 8). According to the shear stress development at the interface, the perfect plastic yield condition was used to calculate the shear stresses. The results indicated a better prediction by the use of the enhanced hypoplastic model. The fact that model did not require any special parameter calibration procedures is an additional advantage. This homogeneous stress field in the soil continuum using the new approach with the hypoplastic model is preferable because this high localisation in such a test device is not observed in experimental studies [58, 46]. Rotta Loria et al. [2] also found that higher pile-soil strength properties lead to higher yield stresses in the soil mass.

5. MODELLING OF LARGE SCALE INTERFACE SHEAR DEVICE

This section emphasises the possibilities of using the new approach in larger boundary value problems. The large interface shear device developed at the Karlsruhe Institute of Technology is introduced and was modelled with the granular enhanced form of the interface constitutive model [35] using the new approach. In addition to the shearing, the filling of the test device was modelled to capture the correct initial stress and deformation field of the large soil sample.

5.1. Modelling large shear device

The large shear device (Figure 9) developed at Karlsruhe Institute of Technology is described by Vogelsang et al. [42] and Rebstock [59]. The main goal of the interface shear device was to designate reliable test data as benchmarks

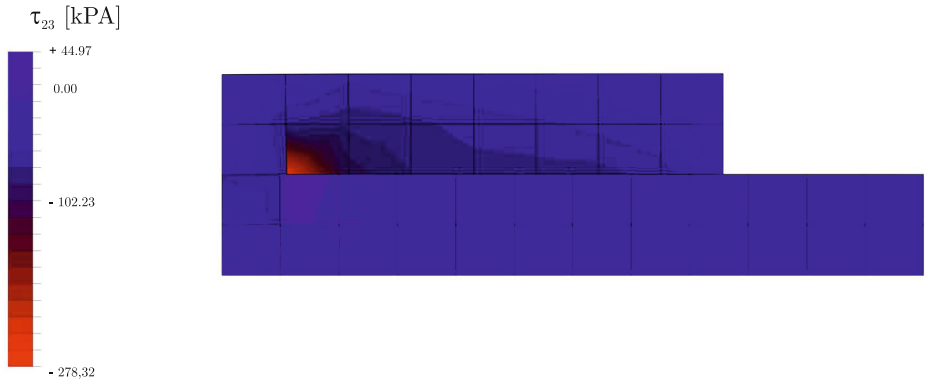

(a) Mohr-Coulomb

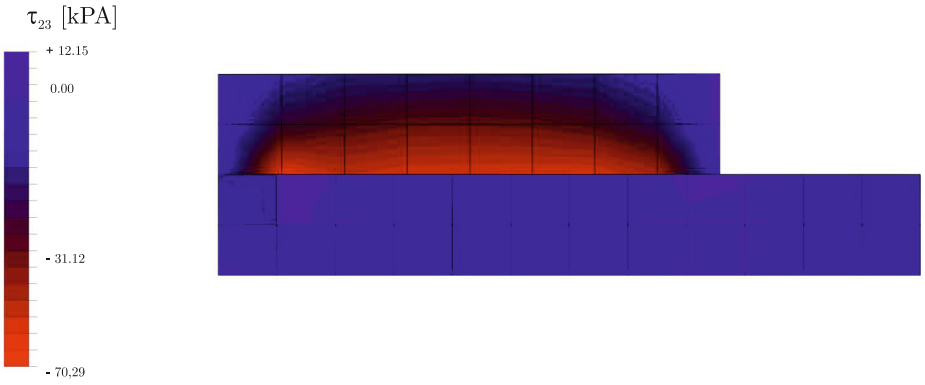

(b) Hypoplastic

Figure 7: Comparison of the shear stress results for the 100 kPa direct interface shear test using the Mohr-Coulomb and hypoplastic interface models

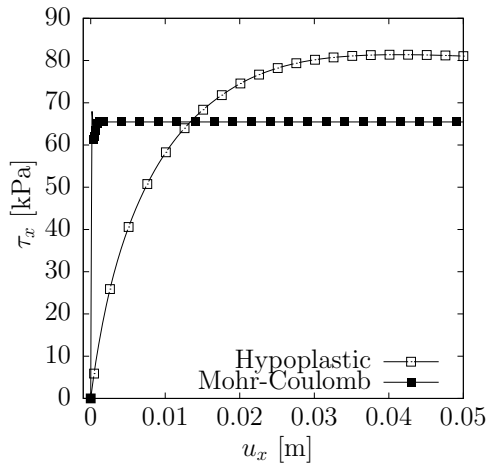

Figure 8: Shear displacement u_x- shear stress τ_x for the comparison of Mohr-Coulomb and hypoplastic interface model

Table 2: Hypoplastic parameters for Karlsruhe sand [55]

φ_c	h_s[kPa]	n	e_{d0}	e_{c0}	e_{i0}	α	β
31	$1 \cdot 10^6$	0.29	0.61	0.96	1.09	0.13	2

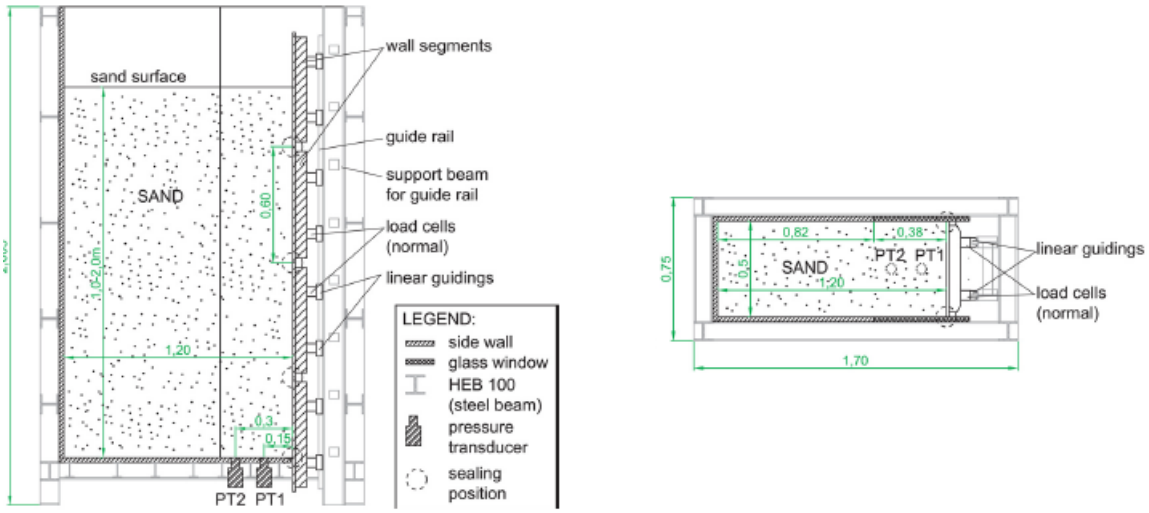

(a) Side view

(b) Top view

Figure 9: Side and top view of the large scale interface shear device from Vogelsang et al. [42]

for numerical models [60]. This data was used in the simulations.
The device can model the installation for various geotechnical engineering structures. It can thus be used as an interface device, to estimate the tip resistance, and for 2D cavity expansion tests. These different problems are important when considering holistic modelling and design in geotechnical engineering.
The soil was modelled with the hypoplasticity model of Von Wolffersdorff [44] using the parameters summarized in Table 2. These parameters were supplement by Vogelsang et al. [60] and differ from the parameters of Karlsruhe Sand [55]. The contact normal behaviour was modelled with an augmented Lagrange approach, which tends to be more stable than a penalty approach [61, 62]. The rough segment was modelled using a completely rough frictional value of $\kappa_r = 1.0$ in the Mohr-Coulomb model $\mu = 1.0$ and a roughness value for the hypoplastic model using the new approach for interface modelling considering taken into consideration 3D soil models.
The stepwise procedure for modelling the filling of the test device was adapted from Vogelsang et al. [60]. The experimental results used for comparison are given by Vogelsang et al. [63].
The procedure described by Vogelsang et al. [60] was important to simulate the initial test stress and deformation state in the device. This modelling technique was able to model filling of the test device. The set-up that was modelled had a soil sample height of 1.50 m. The relative density was $I_D = 0.65$ and the initial void ratio was $e_0 = 0.75$ as indicated by Vogelsang et al. [63]. The filling process was modelled with 10 layers [60].
The modelling procedure (Figure 10) consist out of three steps:

1. A body force that is x times smaller than the normal gravity is applied to the soil sample. This step is necessary to achieve equilibrium with minimal displacements. (**Geostatic**)
2. The gravity is applied stepwise until the final layer n, thereby modelling the filling of the test device. (**Filling**)
3. After the final layer is deposited, the displacement to the wall panels is applied. (**Shearing**)

Figure 11a shows the results of the filling simulation with the Mohr-Coulomb contact model before the shearing. The results of the hypoplastic contact modelling are shown in Figure 11b. The PTE1 and PTE2 sensor positions are shown

in Figure 9. The evolution of vertical stresses is dependent on the filling state. Compared with the hypoplastic model, the Mohr-Coulomb model showed a better agreement for the evolution of the vertical stress σ_z. The relation of the height γh_{sand} and the soil weight is linear. Up to a height of 0.5 m, the earth pressure follows a nearly linear behaviour. After exceeding the filling height of 0.5 m, a non-linear behaviour was observed. The better model behaviour of the enhanced hypoplastic granular interface model can be explained by its more advanced non-linear formulation compared with the simple Mohr-Coulomb model.

The horizontal stress evolution was also given after the complete filling of the device (Figure 12a). The earth pressure distribution for a K_0 value of 0.37, [60] can be used as approximation. The results of the fill modelling using the enhanced hypoplastic contact model yield a slightly better prediction than the Mohr-Coulomb interface model. However, both models slightly overpredicted the horizontal stress at the bottom of the box. Vogelsang et al. [60] mentioned that such a discrepancy can happen because of the low stresses inside the model device. This was in contrast to the higher stresses used to calibrate the hypoplastic model parameters for the Karlsruhe sand [55].

The experimental data showed small jumps in the horizontal stress distribution. These were caused by the transition gap from one segment to another segment and the earth pressure measurement system [60]. In the finite element simulations with a Mohr-Coulomb or enhanced hypoplastic interface constitutive models, these jumps did not exist. This can be justified by the fact that a smooth earth pressure distribution along the wall is expected.

After the fill modelling, the shear phase was simulated (Figure 12b). The model using the Mohr-Coulomb frictional model showed an underprediction compared with the experimental data from Vogelsang et al. [63]. The use of the hypoplastic contact model yielded a better agreement (Figure 12b). The asymptotic value was identical to the experimental value. The general behaviour with the hypoplasticity contact routine was similar to the experimental data. However, a slight difference around the small peak in the experimental data was observed. After the peak point, a small increase of the shear force could be observed. This was not the case for the hypoplastic interface model. This can have various reasons; the initial horizontal stress condition was higher than in the experimental data (Figure 12a). However, the hypoplastic interface model was better than the Mohr-Coulomb model and is preferable. The shear stress by the Mohr-Coulomb model tend to a lower shear stress mobilization then before (Figure 12b). The Mohr-Coulomb model (Figure 13) led to more localised mobilized shear stress zone than an enhanced hypoplastic interface model. In summary, the a more advanced constitutive model for frictional behaviour taking into consideration the volumetric response of the interface led to better predictions. This was shown by fill modelling of the device and shear simulation with the enhanced hypoplastic model. The overburden pressure in the soil sample is smaller than real geotechnical structures (e.g. piles, anchors, and retaining walls).

Comparing the results of the shearing phase (Table 3) it can be seen that under a high shear displacement (−50 mm), the difference in percentage from the experimental to the simulation results is high. In addition to the absolute force values, the volumetric behaviour at the interface is important as indicated by experimental research e.g. [64, 65].

5.2. Remarks and practical implications

Using the new concept for modelling interfaces is an advantage (Figure 7). Taken into consideration the stress field for the direct shear test, a more homogeneous stress field with a less localised response is preferable because a homogeneous mobilisation of the shear stress into the soil mass is expected and has been confirmed [45, 46].

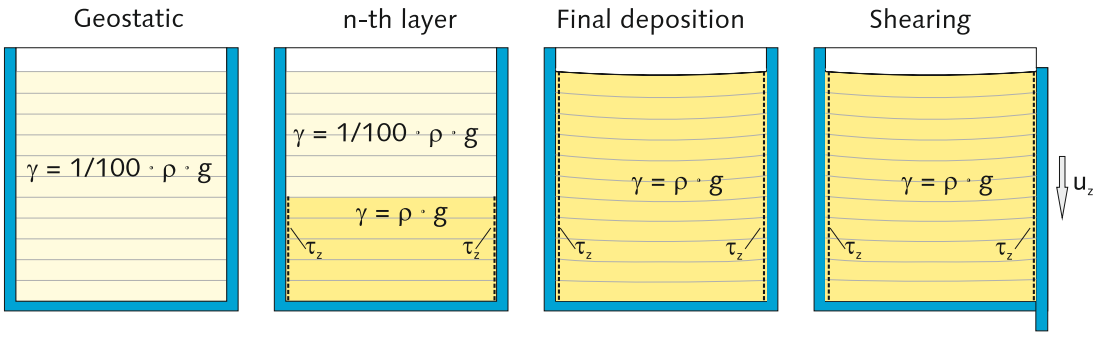

Figure 10: Illustration of the applied calculation process: Modelling filling and shearing of the interface shear device [60]

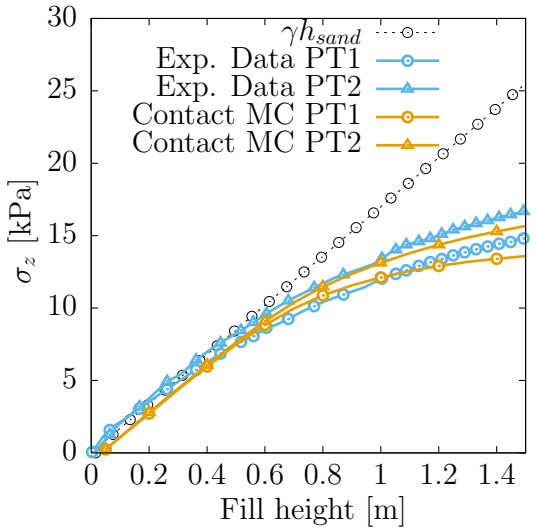

(a) Mohr- Coulomb

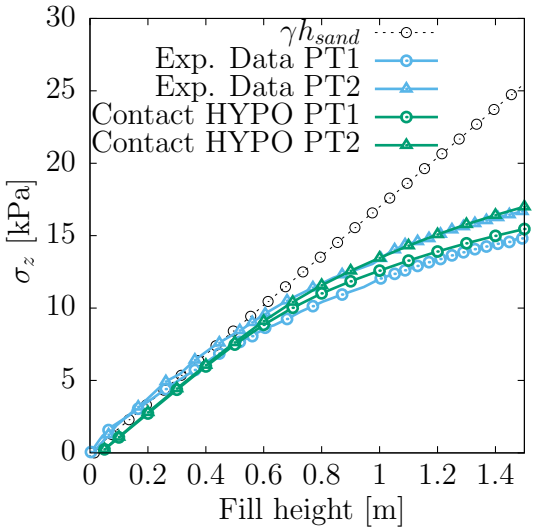

(b) hypoplastic

Figure 11: Vertical stress evolution σ_z [kPa] with increasing filling height [m]

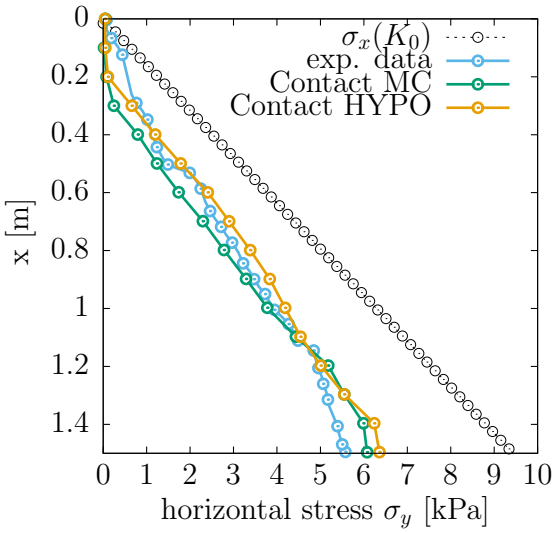

(a) Earth pressure distribution into the ITD device

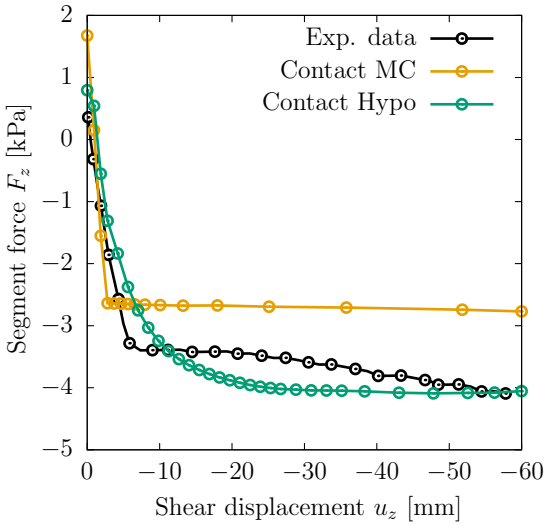

(b) Shear force for the rough panel: Comparison of experimetal data with simulations using the Mohr-Coulomb and hypoplastic interface models

Figure 12: Simulation results for earth pressure distribution (a) and the shear force vs shear displacement results (b)

Table 3: Differences between computed to experimental results for the shearing phase

Shear displacement u_z [mm]	Experimental F_z	Mohr-Coulomb F_z [kPa / %]	Hypoplastic F_z [kPa / %]
-10	-3.3	-0.55 / -17.9	-0.27 / -8.18
-30	-3.8	-1.05 / -27.6	+0.25 / +7.8
-50	-4.2	-1.45 / -34.5	+0.09 / +2.3

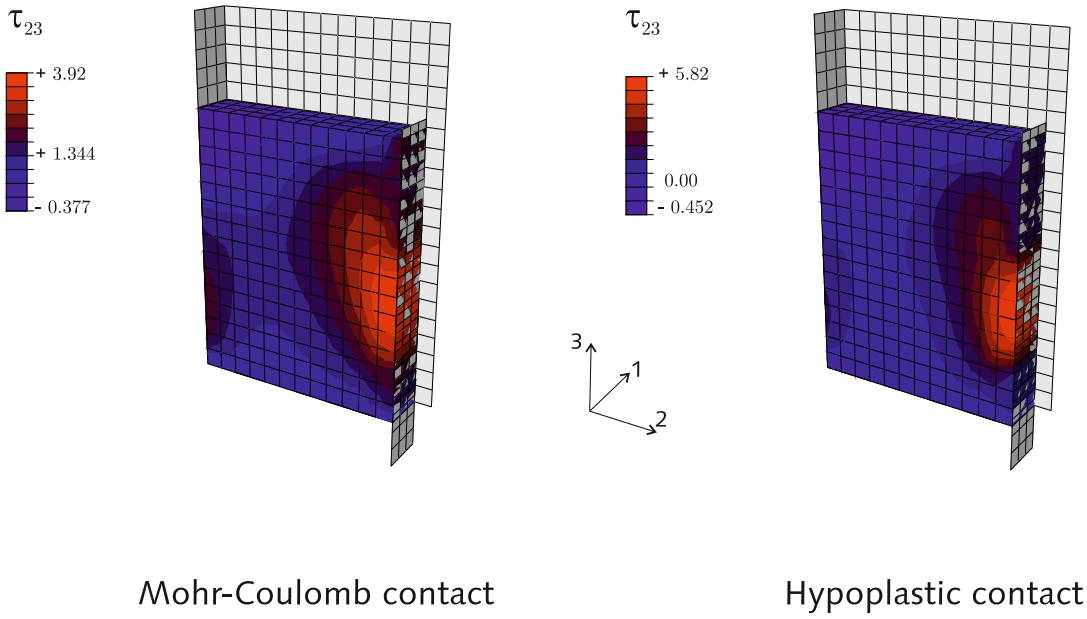

Figure 13: Results for the shear stress σ_{zy} after 60mm shearing. Left side is the Mohr-Coulomb contact and on the right hand side the hypoplastic contact model

With respect to the large interface shear test device, the results (filling of the box) were not improved by using the new concept. However, a better description of the shearing behaviour could be observed. The parameters were not calibrated for the low-stress condition [60]. In addition, the test set-up only takes into consideration one completely rough segment, whereas all other segments are smooth. This is different for full-scale applications.
There are numerous practical implications. The most important is that using the new approach, every constitutive model can be used as an interface model. For a holistic soil-structure interaction simulation, this is possible if the soil and interface use the same model theory. Having achieved this more advanced models for interface modelling, which do not require specialised interface tests in the initial step, can be used. This will allow for the use of advanced interface models for Class-A predictions. Griffiths [66, 67] highlighted that the use of interface modelling techniques as well as special interface constitutive models is important for reliable simulation results, which are readily achieved using the new concept.

6. CONCLUSION

A new approach to modelling interfaces by applying a 3D soil model is presented. The 3D soil model (UMAT) is used as a constitutive driver using reduced tensors for simple shear conditions. These conditions are taken into consideration in the case of reduced stress and strain tensor assuming a simple shear deformation pattern. This reduced stress and strain rate vector is expressed in Voigt notation. The frictional contact is modelled with the FRIC subroutine, and the UMAT can be used as a constitutive driver to eliminate the need for additional models. An additional benefit of the method is that only the code interfaces between the two different subroutines must be ensured; a complete code must not be written. The scheme is explained and can be easily modified for other models or numerical techniques. To overcome the limitations of the surface-to-surface approach for the normal volumetric modelling, a Newton-Raphson scheme is used. The Newton-Raphson algorithm is a stable and robust solution for achieving the correct volumetric behaviour.
The new implementation approach is used to model the constitutive interface models by developed Stutz et al. [35, 37]. The algorithm used in the approach was tested against the Gauss-point algorithm with the simple Euler forward integration results of Stutz et al. [35, 37]. When verifying these models, it was shown that the mesh size has only a

small influence. The approach proposed affords excellent prediction capability. The results were better than expected, but can be explained by the combination of the Newton-Raphson (FRIC) and Runge-Kutta (UMAT) schemes implemented by the user defined subroutines.
Comparing the hypoplastic and Mohr-Coulomb interface model showed that a more realistic stress field was modelled with the hypoplastic models. Finally, a boundary value problem was modelled using the hypoplastic model [44] with the new concept and the Mohr-Coulomb model for interface behaviour. The soil in the boundary value problem is modelled with the hypoplastic model of Von Wolffersdorff [44]. The comparison between the enhanced hypoplastic and Mohr-Coulomb interface model shows a better prediction with the enhanced hypoplastic model. This was expected and is indicated by Said et al. [1] and Rotta Loria et al. [2].
The conclusion from the different boundary value problems shows that the new approach is stable when using the user-defined material subroutine (UMAT) and the user defined frictional constitutive model (FRIC) in the software package ABAQUS. In general, the implementation concept can be applied to other numerical techniques such as zero-thickness [4, 7] or thin-layer interface elements [68]. This could lead to a modification of the approach, but it is possible with major changes to the concept. For example, the node-deformations could be used for normal contact strain calculation, thereby eliminating the need for the Newton-Raphson iteration. Although recently proposed methods [8, 9, 62, 69] are more widely applicable, but the effort for our approach is smaller, and the application more simpler than specialised finite element techniques or technologies. The availability and user-friendly implementation in a suitable finite element software will lead to the use of more advanced interface models.
One of the major advantages of the new implementation concept over specialized interface models is the use of the same parametrisation as the surrounding soil. This enables the use of advanced interface models in Class-A predictions [70]. The only additional parameter that must be estimated or assumed is the roughness coefficient κ_r.
Future work should focus on a continuous detailed verification and validation in addition to the implementation of the method in other numerical techniques.

ACKNOWLEDGEMENT

The second author greatly appreciates financial support by research grant 15-05935S of the Czech Science Foundation. The third author acknowledges the Federal State Funding at Kiel University.

References

[1] I. Said, V. De Gennaro, R. Frank, Axisymmetric finite element analysis of pile loading tests, Computers and Geotechnics 36 (1-2) (2009) 6–19.
[2] A. F. Rotta Loria, F. Orellana, A. Minardi, J.-M. Fürbringer, L. Laloui, Predicting the axial capacity of piles in sand, Computers and Geotechnics 69 (2015) 485–495.
[3] R. E. Goodman, R. L. Taylor, T. L. Brekke, A Model for the mechanics of Jointed rock, Journal of the soil mechanics and foundations division.
[4] G. Beer, An isoparametric joint/interface element for finite element analysis, International Journal for Numerical and Analytical Methods in Geomechanics 21 (1985) 585–600.
[5] F. Belgacem, P. Hild, P. Laborde, The mortar finite element method for contact problems, Mathematical and Computer Modelling 28 (4-8) (1998) 263–271.
[6] H. Stutz, T. Benz, F. Wuttke, Extended zero-thickness interface element for accurate soil pile interaction modelling, in: NUMGE 2014, Delft, The Netherlands, 2014, pp. 283–288.
[7] B. Cerfontaine, A. Dieudonn, J. Radu, F. Collin, R. Charlier, 3d zero-thickness coupled interface finite element: Formulation and application, Computers and Geotechnics 69 (2015) 124 – 140.
[8] C. Weißenfels, P. Wriggers, Methods to project plasticity models onto the contact surface applied to soil structure interactions, Computers and Geotechnics 65 (2015) 187–198.
[9] C. Weißenfels, P. Wriggers, A contact layer element for large deformations, Computational Mechanics 55 (5) (2015) 873–885.
[10] K. A. Fischer, D. Sheng, A. J. Abbo, Modeling of pile installation using contact mechanics and quadratic elements, Computers and Geotechnics 34 (2007) 449–461.
[11] J. Hallquist, NIKE2D: An Implicit, Finite Deformation, Finite Element Code for Analysing of the Static and Dynamic Response of two-dimensional Solids, Tech. rep., UC-Lawrence Livermore National Laboratory (1979).
[12] A. Haraldsson, Formulierung und Simulation der Kontaktvorgänge in der Baugrund-Tragwerk-Interaktion, Ph.D. thesis, Universität Hannover (2004).
[13] M. Nazem, M. Kardani, J. P. Carter, D. Sheng, A comparative study of error assessment techniques for dynamic contact problems of geomechanics, Computers and Geotechnics 40 (2012) 62–73.
[14] M. Nazem, On Application of the Third Medium Contact Method in Analysis of Geotechnical Problems, in: 2nd Austrailian Geomechanics Conference, 2016.

[15] H. Sabetamal, M. Nazem, J. P. Carter, S. W. Sloan, Large deformation dynamic analysis of saturated porous media with applications to penetration problems, Computers and Geotechnics 55 (2014) 117–131.
[16] G. W. Clough, J. M. Duncan, Finite Element Analyses of Retaining Wall Behaviour, Journal of Soil Mechanics and Foundation Division (12) (1971) 1657–1673.
[17] J. E. Gómez, G. M. Filz, R. M. Ebeling, Extended Hyperbolic Model for Sand-to-Concrete Interfaces, Journal of Geotechnical and Geoenvironmental Engineering 129 (11) (2003) 993–1000.
[18] A. Gens, I. Carol, E. Alonso, An interface element formulation for the analysis of soil-reinforcement interaction, Computers and Geotechnics 7 (1988) 133–151.
[19] V. N. Ghionna, G. Mortara, An elastoplastic model for sand - structure interface behaviour, Géotechnique 52 (1) (2002) 41–50.
[20] K. Fakharian, E. Evgin, Elasto-plastic modelling of stress-path dependent behaviour of interfaces, International Journal of Numerical and Analytical Methods in Geomechanics 24 (2000) 183–199.
[21] T. B. Hamid, G. A. Miller, A constitutive model for unsaturated soil interfaces, International Journal for Numerical and Analytical Methods in Geomechanics 32 (13) (2008) 1693–1714.
[22] I. Shahrour, F. Rezaie, An elastoplastic constitutive relation for the soil-structure interface under cyclic loading, Computers and Geotechnics 21 (1) (1997) 21–39.
[23] A. Lashkari, Prediction of the shaft resistance of nondisplacement piles in sand, International Journal for Numerical and Analytical Methods in Geomechanics (January 2012) (2013) 904–931.
[24] H. Liu, E. Song, H. I. Ling, Constitutive modeling of soil-structure interface through the concept of critical state soil mechanics, Mechanics Research Communications 33 (4) (2006) 515–531.
[25] H. Liu, H. I. Ling, Constitutive description of interface behavior including cyclic loading and particle breakage within the framework of critical state soil mechanics, International Journal for Numerical and Analytical Methods in Geomechanics 32 (12) (2008) 1495–1514.
[26] H. Nakayama, Modelling interfaces between sand and structural elements, Ph.D. thesis (2006).
[27] L. Hu, J. L. Pu, Application of damage model for soilstructure interface, Computers and Geotechnics 30 (2) (2003) 165–183.
[28] N. Navayogarajah, C. Desai, P. Kiousis, Hierarchical singlesurface model for static and cyclic behavior of interfaces, Journal of Engineering Mechanics 118 (5) (1992) 990–1011.
[29] R. C. Shao, C. S. Desai, Implementation of DSC model and application for analysis of field pile tests under cyclic loading, International Journal for Numerical and Analytical Methods in Geomechanics 24 (2000) 601–624.
[30] N. C. Samtani, C. S. Desai, L. Vulliet, An interface model to describe viscoplastic behavior, International Journal for Numerical and Analytical Methods in Geomechanics 20 (March 1995) (1996) 231–252.
[31] J. Liu, D. Zou, X. Kong, A three-dimensional state-dependent model of soil-structure interface for monotonic and cyclic loadings, Computers and Geotechnics 61 (2014) 166–177.
[32] V. Gennaro, R. Frank, Elasto-plastic analysis of the interface behaviour between granular media and structure, Computers and Geotechnics 29 (7) (2002) 547–572.
[33] S. Costa D Aguiar, A. Modaressi-Farahmand-Razavi, J. A. dos Santos, F. Lopez-Caballero, Elastoplastic constitutive modelling of soilstructure interfaces under monotonic and cyclic loading, Computers and Geotechnics 38 (4) (2011) 430–447.
[34] M. Arnold, I. Herle, Hypoplastic description of the frictional behaviour of contacts, Numerical Methods in Geotechnical Engineering (2006) 101–106.
[35] H. Stutz, D. Mašín, F. Wuttke, Enhancement of a hypoplastic model for granular soil-structure interface behaviour, Acta Geotechnica.
[36] J. Duriez, . Vincens, Constitutive modelling of cohesionless soils and interfaces with various internal states: An elasto-plastic approach, Computers and Geotechnics 63 (2015) 33 – 45.
[37] H. Stutz, D. Mašín, Hypoplastic interface model for fine-grained soils, International Journal of Analytical and Numerical Methods in Geomechanicsdoi:10.1002/nag.2561.
[38] Hibbit, Karlsson, Sorensen, Abaqus version 6.14 (2015).
[39] M. Boulon, Basic Features Of Soil Structure Interface Behaviour, Computers and Geotechnics 7 (1-2) (1989) 115–131.
[40] M. Boulon, R. Nova, Modelling of soil structure interface behavior a comparison between elastoplastic and rate type laws, Computers and Geotechnics 9 (1990) 21–46.
[41] H. Stutz, D. Mašín, Prädel, F. Wuttke, Thermo-mechanical hypoplastic interface model for fine-grained soils, in: Wuttke, Bauer, Sanchez (Eds.), Energy geotechnics, 2016, pp. 351–357. doi:10.1201/b21938-56.
[42] J. Vogelsang, G. Huber, T. Triantafyllidis, A Large-Scale Soil-Structure Interface Testing Device, Geotechnical Testing Journal 36 (5) (2013) 1–13.
[43] D. Mašín, Clay hypoplasticity with explicitly defined asymptotic states, Acta Geotechnica 8 (2013) 481–496.
[44] P. A. von Wolffersdorff, Hypoplastic relation for granular materials with a predefined limit state surface, Mechanics of Cohesive-Frictional Materials 1 (3) (1996) 251–271.
[45] J. T. DeJong, D. J. White, M. Randolph, Microscale oberservation and modeling of soil-structure interface behavior using particle image velocimetry, Soils and Foundations.
[46] J. T. DeJong, Z. J. Westgate, Role of Initial State, Material Properties, and Confinement Condition on Local and Global Soil-Structure Interface Behavior, Journal of Geotechnical and Geoenvironmental Engineering 135 (11) (2009) 1646–1660.
[47] G. Gudehus, A Comprehensive Constitutive Equation For Granular Materials, Soils and Foundations 36 (1) (1996) 1–12.
[48] D. Mašín, Hypoplastic Cam-clay model, Géotechnique 62 (6) (2012) 549–553.
[49] H. Matsuoka, T. Nakai, Stressdeformation and strength characteristics of soil under three different principal stresses., in: Proceedings of the Japanese Society of Civil Engineers, vol 232, 1974, pp. 59–70.
[50] Hibbit, Karlsson, Sorensen, ABAQUS/Standard Analysis User's Manual, Hibbit, Karlsson, Sorensen Inc., USA, 2015.
[51] G. Gudehus, A. Amorosi, A. Gens, I. Herle, D. Kolymbas, D. Ma????n, D. M. Wood, A. Niemunis, R. Nova, M. Pastor, C. Tamagnini, G. Viggiani, The soilmodels.info project, International Journal for Numerical and Analytical Methods in Geomechanics 32 (12) (2008) 1571–1572.

[52] S. Gutjahr, Optimierte Berechnung von nicht gestützten Baugrubenwänden in Sand, Tu dortmund heft 25 (2003).
[53] M. Arnold, Hypoplastische Beschreibung zweidimensionaler Reibungskontakte, in: Technische Universität Dresden, Mitteilungen Institut für Geotechnik, Heft 15, Ohde-Kolloquium 2005, 2005, pp. 69–86.
[54] M. Arnold, Personal communication (2016).
[55] I. Herle, G. Gudehus, Determination of parameters of a hypoplastic constitutive model from properties of grain assemblies, Mechanics of cohesive -Frictional Materials 4 (1999) 461–486.
[56] E. Wernick, Skin Friction of Cyclindrical Anchors in Non-Cohesive Soils, in: Symposium on Soil Reinforcing and Stabilising Techniques, 1978.
[57] J. T. Tabucanon, D. W. Airey, H. G. Poulos, Pile Skin Friction in Sand from Constant Normal Stiffness Test, Geotechnical Testing Journal Vol. 18 (1995) 350–364.
[58] J. De Jong, M. Randolph, D. White, Interface load transfer degradation during cyclic loading: a microscale investigation, Soils and Foundations 43 (4) (2003) 81–93.
[59] D. Rebstock, Verspannung und Entspannung von Sand entlang von Baukörpern, Ph.D. thesis, Karlsruher Institut für Technologie (KIT) (2011).
[60] J. Vogelsang, H. Zachert, G. Huber, T. Triantafyllidis, Effects of soil deposition on the intial stress state in model tests: Experimental results and FE simulation, in: Th. Triantafyllidis (Ed.), Holistic Simulation of Geotechnical Installation Processes, Lecture Notes in Applied and Computational Mechanics 77, Vol. 77, Springer International Publishing Switzerland, 2015, pp. 1–20.
[61] M. A. Puso, T. A. Laursen, J. Solberg, A segment-to-segment mortar contact method for quadratic elements and large deformations, Computer Methods in Applied Mechanics and Engineering 197 (68) (2008) 555–566.
[62] P. Dziewiecki, C. Weißenfels, P. Wriggers, Modelling of soil structure interaction by applying a hypoplastic material behaviour within mortar contact formulation, in: Th. Triantafyllidis (Ed.), Holistic Simulation of Geotechnical Installation Processes, Lecture Notes in Applied and Computational Mechanics 77, Vol. 77, Springer International Publishing Switzerland, 2015, pp. 59–72.
[63] J. Vogelsang, G. Huber, T. Triantafyllidis, Demonstrator Experiments on significant effects during pile installation, in: Th. Triantafyllidis (Ed.), Holistic Simulation of Geotechnical Installation Processes, Lecture Notes in Applied and Computational Mechanics 77, Vol. 77, Springer International Publishing Switzerland, 2015, pp. 1–20.
[64] B. M. Lehane, D. J. White, Lateral stress changes and shaft friction for model displacement piles in sand, Canadian Geotechnical Journal 42 (4) (2005) 1039–1052.
[65] D. J. White, M. D. Bolton, Displacement and strain paths during plane-strain model pile installation in sand, Géotechnique 54 (6) (2004) 375–397. doi:10.1680/geot.2004.54.6.375.
[66] D. Griffiths, Numerical modelling of interfaces using conventional finite elements, in: Fifth International Conference on Numerical Methods in Geomechanics, Nagoya, 1985, pp. 837–843.
[67] D. Griffiths, Numerical studies of soil-structure interaction using a simple interface model, Canadian Geotechnical Journal 25 (1988) 158–162.
[68] C. S. Desai, M. M. Zaman, J. G. Lightner, H. J. Siriwardane, Thin-layer element for interfaces and joints, International Journal for Numerical and Analytical Methods in Geomechanics 8 (1984) 19–43.
[69] M. Zhou, B. Zhang, C. Peng, W. Wu, Three-dimensional numerical analysis of concrete-faced rockfill dam using dual-mortar finite element method with mixed tangential contact constraints, International Journal for Numerical and Analytical Methods in Geomechanics-doi:10.1002/nag.2524.
[70] T. W. Lambe, Predictions in soil engineering, Gotechnique 23 (2) (1973) 151–202.
[71] E. Bauer, Calibration of a Comprehensive hypoplastic model for granular materials, Soils and Foundations 36 (1996) 13–26.
[72] D. Mašín, A hypoplastic constitutive model for clays, International Journal for Numerical and Analytical Methods in Geomechanics 29 (2005) 311–336.
[73] D. Mašín, N. Khalili, A thermo-mechanical model for variably saturated soils based on hypoplasticity, International Journal for Numerical and Analytical Methods in Geomechanics 36 (2012) 1461–1485.
[74] D. Mašín, Clay hypoplasticity model including stiffness anisotropy, Géotechnique 2 (3) (2014) 232–238.
[75] J. Jaky, Pressure in silos, in: 2nd ICSMFE, 1948, pp. 103–107.

Appendix A. Redefined mathematical operators by [35]

The modelling approach was introduced by Stutz et al. [35]. By preserving the continuum constitutive models, the redefined tensorial operators in combination with the reduced stress Equations (2) and strain rate vectors Equations (4) used, to simulate the interface behaviour.
The *Voigt* notation is used to reduce the second order and fourth order tensors into vectors and matrices. The first rank tensors $\boldsymbol{X}$ and $\boldsymbol{Y}$ and the second rank tensor $\mathcal{S}$ are defined as:

$$\boldsymbol{X} = \begin{bmatrix} X_1 \\ X_2 \\ X_3 \\ X_4 \end{bmatrix} \quad \boldsymbol{Y} = \begin{bmatrix} Y_1 \\ Y_2 \\ Y_3 \\ Y_4 \end{bmatrix} \quad \mathcal{S} = \begin{bmatrix} S_{11} & S_{12} & S_{13} & S_{14} \\ S_{21} & S_{22} & S_{23} & S_{24} \\ S_{31} & S_{32} & S_{33} & S_{34} \\ S_{41} & S_{42} & S_{43} & S_{44} \end{bmatrix} \tag{A.1}$$

The trace of $\boldsymbol{X}$ is defined as:

$$tr\,(\boldsymbol{X}) = X_1 + 2X_2 \tag{A.2}$$

The Euclidean norm $\boldsymbol{X}$ is:

$$\|\boldsymbol{X}\| = \sqrt{\boldsymbol{X} : \boldsymbol{X}} \tag{A.3}$$

The determinant of $\boldsymbol{X}$ is defined as:

$$\det(\boldsymbol{X}) = \mathbf{1} : \boldsymbol{X} = X_1 X_2^2 - X_4^2 X_2 - X_3^2 X_2 \tag{A.4}$$

The second-order unity tensor is defined as:

$$\mathbf{1} = \begin{bmatrix} 1 \\ 1 \\ 0 \\ 0 \end{bmatrix} \tag{A.5}$$

The fourth order unity tensor is:

$$\boldsymbol{I} = \begin{bmatrix} 1 & 0 & 0 & 0 \\ 0 & 0.5 & 0 & 0 \\ 0 & 0 & 0.5 & 0 \\ 0 & 0 & 0 & 0.5 \end{bmatrix} \tag{A.6}$$

The deviator from $\boldsymbol{X}$ is written as:

$$\boldsymbol{X}^* = \boldsymbol{X} + \mathbf{1}\left(\frac{-tr\boldsymbol{X}}{3}\right) = \begin{bmatrix} \frac{2}{3}X_1 - \frac{2}{3}X_2 \\ \frac{X_2}{3} - \frac{X_1}{3} \\ X_3 \\ X_4 \end{bmatrix} \tag{A.7}$$

The normalized deviator from $\boldsymbol{X}$ is defined as:

$$\hat{\boldsymbol{X}}^* = \frac{\boldsymbol{X}}{tr\boldsymbol{X}} - \frac{\mathbf{1}}{3} = \begin{bmatrix} \frac{X_1}{X_1 + 2X_2} - \frac{1}{3} \\ \frac{X_2}{X_1 + 2X_2} - \frac{1}{3} \\ \frac{X_3}{X_1 + 2X_2} \\ \frac{X_4}{X_1 + 2X_2} \end{bmatrix} \tag{A.8}$$

The inner product $(\cdot)$ is defined as:

$$\boldsymbol{X} \cdot \boldsymbol{Y} = \begin{bmatrix} X_1 Y_1 + X_3 Y_3 + X_4 Y_4 \\ X_2 Y_2 + X_3 Y_3 \\ X_1 Y_3 + X_3 Y_2 \\ X_4 Y_1 + X_2 Y_4 \end{bmatrix} \tag{A.9}$$

The double inner product (:) between the two first-rank tensors is:

$$\boldsymbol{X} : \boldsymbol{Y} = X_1 Y_1 + 2X_2 Y_2 + 2X_3 Y_3 + 2X_4 Y_4 \tag{A.10}$$

The double inner product (:) between second-rank and first-rank tensors reads:

$$\mathcal{S} : \boldsymbol{Y} = \begin{bmatrix} S_{11} Y_1 + 2S_{12} Y_2 + 2S_{13} Y_3 + 2S_{14} Y_4 \\ S_{21} Y_1 + 2S_{22} Y_2 + 2S_{23} Y_3 + 2S_{24} Y_4 \\ S_{31} Y_1 + 2S_{32} Y_2 + 2S_{33} Y_3 + 2S_{34} Y_4 \\ S_{41} Y_1 + 2S_{42} Y_2 + 2S_{43} Y_3 + 2S_{44} Y_4 \end{bmatrix} \tag{A.11}$$

Finally, the outer product $(\otimes)$ is:

$$\boldsymbol{X} \otimes \boldsymbol{Y} = \begin{bmatrix} X_1 Y_1 & X_1 Y_2 & X_1 Y_3 & X_1 Y_4 \\ X_2 Y_1 & X_2 Y_2 & X_2 Y_3 & X_2 Y_4 \\ X_3 Y_1 & X_3 Y_2 & X_3 Y_3 & X_3 Y_4 \\ X_4 Y_1 & X_4 Y_2 & X_4 Y_3 & X_4 Y_4 \end{bmatrix} \tag{A.12}$$

Appendix B. Hypoplastic granular model of Von Wolffersdorff [44]

The general form of the hypoplastic model formulation [47] can be written as:

$$\dot{\boldsymbol{T}} = f_s \left(\boldsymbol{L} : \boldsymbol{D} + f_d \boldsymbol{N} \|\boldsymbol{D}\| \right) \tag{B.1}$$

where $\dot{\boldsymbol{T}}$ and $\boldsymbol{D}$ are the objective stress rate and stretching tensor, respectively. $\boldsymbol{N}$ and $\boldsymbol{L}$ are the fourth- and second-order constitutive tensors. f_s is the barotropy factor controlling the influence of the mean stress, and f_d is the pyknotropy factor taking into consideration the influence of the relative density.
Von Wolffersdorff [44] extended the basic form of the model by incorporating a predefined limit state surface according to Matsuoka and Nakai [49]. The second order constitutive tensor $\boldsymbol{L}$ is then defined as:

$$\boldsymbol{L} = f_s \frac{1}{\hat{\boldsymbol{T}} : \hat{\boldsymbol{T}}} \left(F^2 \boldsymbol{I} + a^2 \hat{\boldsymbol{T}} \otimes \hat{\boldsymbol{T}} \right) \tag{B.2}$$

where $\hat{\boldsymbol{T}} = \boldsymbol{T} / \operatorname{tr} \boldsymbol{T}$ is a deviator stress and $\boldsymbol{I}$ is the fourth order unity tensor. The coefficient a is defined as:

$$a = \frac{\sqrt{3} \left(3 - \sin \varphi_c\right)}{2 \sqrt{2} \sin \varphi_c} \tag{B.3}$$

where ϕ_c is a model parameter. The Matsuoka-Nakai condition is given by the following scalar coefficient as:

$$F = \sqrt{\frac{1}{8} \tan^2 \psi + \frac{2 - \tan^2 \psi}{2 + \sqrt{2} \tan \psi \cos 3\theta}} - \frac{1}{2 \sqrt{2}} \tan \psi \tag{B.4}$$

with the Lode angle θ,

$$\cos 3\theta = -\sqrt{6} \frac{\operatorname{tr} \left(\hat{\boldsymbol{T}}^* \cdot \hat{\boldsymbol{T}}^* \cdot \hat{\boldsymbol{T}}^* \right)}{\left[\hat{\boldsymbol{T}}^* : \hat{\boldsymbol{T}}^* \right]^{3/2}} \tag{B.5}$$

where $\hat{\boldsymbol{T}}^* = \hat{\boldsymbol{T}} - \frac{1}{3}\boldsymbol{1}$ is a deviator stresses and $\tan \psi = \sqrt{3} \|\hat{\boldsymbol{T}}^*\|$. The fourth-order constitutive tensor is defined as:

$$\boldsymbol{N} = f_s f_d \frac{a \cdot F}{\hat{\boldsymbol{T}} : \hat{\boldsymbol{T}}} \left(\hat{\boldsymbol{T}} + \hat{\boldsymbol{T}}^* \right) \tag{B.6}$$

The barotropy factor f_s controls the influence of the mean stress and is given as:

$$\begin{aligned} f_s = & \frac{h_s}{n} \left(\frac{e_i}{e} \right)^{\beta} \frac{1 + e_i}{e_i} \left(\frac{-\operatorname{tr} (\boldsymbol{T})}{h_s} \right)^{1-n} \\ & \cdot \left[3 + a^2 - a \sqrt{3} \left(\frac{e_{i0} - e_{d0}}{e_{c0} - e_{d0}} \right)^{\alpha} \right]^{-1} \end{aligned} \tag{B.7}$$

The pyknotropy factor f_d controls the influence of the relative density, i.e.,

$$f_d = \left(\frac{e - e_d}{e_c - e_d} \right)^{\alpha} \tag{B.8}$$

where e_d,e_c,e_i are limiting void ratios. Under increasing mean pressure, they decrease until the limiting values e_{d0}, e_{c0}, e_{i0} are reached [71].

$$\frac{e_d}{e_{d0}} = \frac{e_c}{e_{c0}} = \frac{e_i}{e_{i0}} = \exp \left[- \left(\frac{\operatorname{tr} (\boldsymbol{T})}{h_s} \right)^n \right] \tag{B.9}$$

Appendix C. Fine-grained hypoplastic model by Mašín [43]

Based on the clay hypoplasticity model given in Mašín [72] with explicitly defined asymptotic states [43], the corresponding interface model is derived by using the reduced stress and strain tensors as shown in Equation (2) and Equation (4). The model uses the general formulation of hypoplasticity with explicitly defined asymptotic states [43] (Equation (6)), f_d^A describes the value of f_d at the asymptotic state boundary surface (ASBS) and $\boldsymbol{d}$ is the asymptotic strain rate direction. Here, $\boldsymbol{A}$ is

$$\boldsymbol{A} = f_s \boldsymbol{L} + \frac{\boldsymbol{\sigma}}{\lambda^*} \otimes \mathbf{1} \tag{C.1}$$

where λ^* is a model parameter. Equation (6) enables the use and incorporation of any appropriate arbitrary shape of the asymptotic shape boundary surface by specifying the dependence of f_d^A on the void and stress ratio [73]. The barotropy factor f_s is calculated using:

$$f_s = \frac{3p}{2}\left(\frac{1}{\lambda^*} + \frac{1}{\kappa^*}\right)\frac{1-2\nu}{1+\nu} \tag{C.2}$$

Equation (C.1) is used to further establish the hypoplastic fine-grained interface models. The $\boldsymbol{L}$ tensor which represents isotropic elasticity, is given by

$$\boldsymbol{L} = \boldsymbol{I} + \frac{\nu}{1-2\nu}\mathbf{1} \otimes \mathbf{1} \tag{C.3}$$

$$f_d = \left(\frac{2p}{p_e}\right)^{\alpha_f} \tag{C.4}$$

The exponent α_f controls the irreversible deformation inside the ASBS. Mašín suggests using α_f [72, 74], which leads to a better prediction of the model response. Additionally, α_f can be treated as an independent parameter [72] to control the non-linear response inside the ASBS.

$$\alpha_f = \frac{ln\left(\frac{\lambda^* - \kappa^*}{\lambda^* + \kappa^*}\left(\frac{3 + a_f^2}{a_f\sqrt{3}}\right)\right)}{ln\,(2)} \tag{C.5}$$

where a_f is

$$a_f = \frac{\sqrt{3}\,(3 - \sin\phi_c)}{2\sqrt{2}\sin\phi_c} \tag{C.6}$$

The factor f_d^A is the limiting value of f_d at the ASBS i.e.

$$f_d^A = 2^{\alpha_f}\,(1 - F_m)^{\alpha_f/\omega} \tag{C.7}$$

The Matsuoka-Nakai factor F_m [49] is:

$$F_m = \frac{9I_3 + I_1 I_2}{I_3 + I_1 I_2} \tag{C.8}$$

using the following invariants:

$$I_1 = tr\boldsymbol{\sigma} \qquad I_2 = \frac{1}{2}\left[\boldsymbol{\sigma} : \boldsymbol{\sigma} - (I_1)^2\right] \qquad I_3 = \det\boldsymbol{\sigma} \tag{C.9}$$

$$\omega = -\frac{ln\left(\cos^2\phi_c\right)}{ln\,(2)} + a_f\left(F_m - \sin^2\phi_c\right) \tag{C.10}$$

with the Lode angle θ,

$$\cos 3\theta = -\sqrt{6}\frac{tr\,(\hat{\boldsymbol{\sigma}}^* \cdot \hat{\boldsymbol{\sigma}}^* \cdot \hat{\boldsymbol{\sigma}}^*)}{[\hat{\boldsymbol{\sigma}}^* : \hat{\boldsymbol{\sigma}}^*]^{3/2}} \tag{C.11}$$

The asymptotic strain rate direction $\boldsymbol{d}$ is given as:

$$\boldsymbol{d} = \frac{\boldsymbol{d}^A}{||\boldsymbol{d}^A||} \tag{C.12}$$

where $\boldsymbol{d}^A$ is written as:

$$\boldsymbol{d}^A = -\hat{\boldsymbol{\sigma}}^* + \mathbf{1}\left[\frac{2}{3} - \frac{1}{4}F_m^{1/4}\right]\frac{F_m^{\xi/2} - \sin^{\xi}\phi_c}{1 - \sin^{\xi}\phi_c} \tag{C.13}$$

The factor ξ controls the ratio of volumetric to shear strain; this factor was obtained using an optimisation procedure to ensure that the strain rate direction satisfies the Jaky formula [75]:

$$\xi = 1.7 + 3.9\sin^2\phi_c \tag{C.14}$$